9-23-2020

A Century of Observations Reveals Increasing Likelihood of Continental-Scale Compound Dry-Hot Extremes

Mohammad Reza Alizadeh
McGill University

Jan Adamowski
McGill University

Mohammad Reza Nikoo
Shiraz University

Amir AghaKouchak
University of California, Irvine

Philip Dennison
University of Utah

See next page for additional authors

CLIMATOLOGY

A century of observations reveals increasing likelihood of continental-scale compound dry-hot extremes

Mohammad Reza Alizadeh[1], Jan Adamowski[1], Mohammad Reza Nikoo[2], Amir AghaKouchak[3,4], Philip Dennison[5], Mojtaba Sadegh[6]*

Using over a century of ground-based observations over the contiguous United States, we show that the frequency of compound dry and hot extremes has increased substantially in the past decades, with an alarming increase in very rare dry-hot extremes. Our results indicate that the area affected by concurrent extremes has also increased significantly. Further, we explore homogeneity (i.e., connectedness) of dry-hot extremes across space. We show that dry-hot extremes have homogeneously enlarged over the past 122 years, pointing to spatial propagation of extreme dryness and heat and increased probability of continental-scale compound extremes. Last, we show an interesting shift between the main driver of dry-hot extremes over time. While meteorological drought was the main driver of dry-hot events in the 1930s, the observed warming trend has become the dominant driver in recent decades. Our results provide a deeper understanding of spatiotemporal variation of compound dry-hot extremes.

INTRODUCTION

Traditional climate risk analyses have focused on the hazardous/anomalous states of one variable at a time (*1*). For example, studies have shown that heatwave magnitudes, frequencies, intensities, and spatial extents are increasing over many regions (*2*), a trend that is projected to continue in a warming climate (*3*). Moreover, analyses of historical precipitation, streamflow, and soil moisture indices show an increasing trend of aridity over many regions around the globe (*4*), and model simulations point to an increasing drought hazard in the 21st century. These extreme events can individually cause significant adverse impacts; however, their concurrence can be even more devastating (*5*, *6*). For example, the compounding effects of drought and hot temperatures can significantly increase tree mortality, which, in turn, may cascade into other hazards, such as wildfires (*7*). Concurrent drought and heatwaves are the most damaging climatic stressors to wheat production with grave implications for global food security; they can also jeopardize electric grid reliability and adversely affect a wide range of natural and built systems (*8*). In the United States alone, three concurrent drought and heatwave events between 2011 and 2013 caused damages equaling roughly 60 billion U.S. dollars (USD).

Compound extremes are typically characterized by a complex chain of interdependent processes at different spatial and temporal scales (*9*). Droughts and heatwaves, for example, are typically initiated by similar synoptic circulation anomalies; however, local- and regional-scale land-atmosphere feedbacks drive the evolution of compound drought-heatwave events and intensify both extremes (*10*). While the probability of multiple extremes occurring simultaneously or successively has historically been low, climate change has systematically altered the relationships between natural hazard drivers, increasing the probability of their concurrence and/or succession as well as their severity and magnitude (*9*, *11*). Background warming due to anthropogenic emissions, for example, triggers earlier initiation of and stronger land-atmosphere feedback loops and extends their spatial impact across North America (*12*), which can, in turn, intensify compound drought-heatwave extremes and spread their spatial extent. The literature shows more frequent compound extremes in recent decades across the entire globe (*13*). Across the contiguous United States (CONUS), concurrent droughts and heatwaves have increased with a statistically significant shift in their distribution between 1990 and 2010 and 1960 and 1980 (*14*). In addition, concurrent moderate droughts and heatwaves have increased across portions of India (*15*), and meteorological droughts are associated with a faster warming rate than the average climate over southern and northeastern United States (*16*).

Land-atmosphere feedbacks can intensify drought-heatwave extremes through two mechanisms: self-intensification and self-propagation (*17*). Self-intensification refers to droughts and heatwaves intensifying one another, and self-propagation refers to the spreading of droughts and heatwaves from one region to downwind regions (*10*, *18*). Previous examinations of compound hot-dry events (and their derivatives, i.e., compound drought-heatwave events) have focused on synoptic circulation patterns that initiate these extremes and self-intensifying land-atmosphere processes that drive the evolution of these events (*1*, *13*, *16*). Here, we examine a less explored mechanism of land-atmosphere feedbacks that explains propagation of terrestrially sourced atmospheric moisture deficit and heat from one region to its neighboring areas, i.e., self-propagation. This process, as manifested through trends in the spatial homogeneity—connectedness—of concurrent dry-hot extremes, has received less attention in past studies. We analyze spatial homogeneity of compound dry-hot extremes over CONUS using more than a century of ground observation climatic data. Further, most of the literature only analyzes the concurrence of droughts and heatwaves after 1950s (*14*, *15*, *19*), which overlooks the megadrought of the 1930s (*13*). We extend the analysis to 1896–2017 (122 years) and provide a new perspective into the temporal trends of compound dry-hot events.

We use monthly precipitation and average temperature observations at the climate division scale to derive annual precipitation (water year - WY: October to September), spring-summer (March

[1]Department of Bioresource Engineering, McGill University, 21111 Lakeshore Road, Ste-Anne-de-Bellevue, QC H9X 3V9, Canada. [2]Department of Civil and Environmental Engineering, College of Engineering, Shiraz University, Shiraz 7134851156, Iran. [3]Department of Civil and Environmental Engineering, University of California, Irvine, 4130 Engineering Gateway, Irvine, CA 92697, USA. [4]Department of Earth System Science, University of California, Irvine, 3200 Croul Hall Irvine, CA 92697, USA. [5]Department of Geography, University of Utah, 260 S Central Campus Dr, Rm 4625, Salt Lake City, UT 84112, USA. [6]Department of Civil Engineering, Boise State University, 1910 University Drive, Boise, ID 83725-2060, USA.
*Corresponding author. Email: mojtabasadegh@boisestate.edu

to August) precipitation, average annual WY temperature, and average spring-summer (March to August) temperature, which are, in turn, used in an empirical copula framework to calculate the joint probability and return period of compound dry-hot years and various subannual events. We define compound dry-hot extremes as years with joint return periods of precipitation deficit and heat excess of longer than 25 years (joint annual exceedance probability of less than 0.04), unless otherwise stated. Joint return period is estimated using the "AND" hazard scenario (drier than a threshold AND hotter than a threshold) in a multivariate framework (*20*). Our results show that the frequency of compound dry-hot extremes is increasing across CONUS, a trend that is significant at the 5% level over the western United States and parts of the northeastern and southeastern United States. These compound extremes are enlarging homogeneously as demonstrated by spatial correlation analysis; i.e., the connectedness of the impacted areas is increasing. This has significant socio-environmental repercussions as larger and more intense extreme events can rapidly deplete regional and national relief resources. This knowledge can help assess regional-to-continental vulnerabilities of natural and built systems under climate change and inform adaptation and mitigation efforts to curb the grave compounding impacts of multiple extremes (*21*).

RESULTS

Temporal trends in precipitation and temperature over CONUS

Nonparametric Mann-Kendall analysis shows a statistically significant increasing trend for the mean annual temperature between 1896 and 2017 (Fig. 1B and fig. S2B) across much of CONUS except for portions of the Southeast, east of the Southern Great Plains, and the southern part of the Midwest. A relatively similar trend exists for mean spring-summer (March to August) temperatures, although it is less pronounced for portions of the Northern Great Plains and Midwest (fig. S1B). Statistically significant trends for annual precipitation, however, are much less pronounced across CONUS (Fig. 1A). Annual precipitation has not changed significantly over much of CONUS, although precipitation patterns and intensities may have shifted. Only a strip of land extending from eastern Texas to the Great Lakes and the Northeast has a statistically significant increasing trend (at the 5% level) for annual precipitation (Fig. 1A and fig. S2A). Trend analysis of precipitation at the annual scale, however, might be contentious in the presence of autocorrelation among successive annual precipitation values when there are persistent multiyear dry periods (*22*). However, further investigation shows that lag-1 autocorrelation values between annual precipitation—and also spring-summer precipitation—generally do not reach statistical significance (fig. S4) to justify removal of autocorrelation before trend analysis. Similar behavior is observed for higher lag values.

While trends in both precipitation and temperature have significant socio-environmental implications, their interdependence can intensify the impacts of the anomalous state of each driver (*11*). For example, extreme temperatures can induce "flash droughts" with devastating impacts such as causing large wildfires (*23*, *24*). Pearson linear correlation analysis shows significant negative association between annual precipitation and mean annual temperature (fig. S5A) across much of the Great Plains and Southwest. This correlation is, however, not statistically significant at the 5% level for the west coast and much of the Pacific Northwest, as well as the Southeast, Northeast, and Midwest. The interdependence is further pronounced between annual precipitation and mean spring-summer (March to August) temperature (fig. S5B) as well as maximum spring-summer temperature (fig. S5C).

Climate change can alter the dependence structure between precipitation and temperature at different spatial and temporal scales (*19*). Arguably, the change in their association might be more important than the change (e.g., increasing trend) in each variable. Given that mean annual temperature, unlike annual precipitation, shows a statistically significant trend across much of CONUS, we linearly detrended the mean annual (as well as mean and maximum spring-summer) temperature and reanalyzed the linear association between temperature and precipitation. Our results point to a more pronounced Pearson correlation coefficient between annual precipitation and mean annual temperature (fig. S6A), when temperature time series are linearly detrended. A similar conclusion holds when temperature is exponentially detrended (fig. S7). This shows that climate change has weakened the association between temperature and precipitation at the annual scale cross CONUS. This finding seems counterintuitive at first glance, as background warming is believed to have strengthened land-atmosphere feedbacks (*12*). A closer look, however, shows that detrending strengthens the correlation between annual precipitation and mean spring-summer temperature (figs. S5B, S6B, and S7B), as well as maximum spring-summer temperature (figs. S5C, S6C, and S7C), which confirms the strengthening of land-atmosphere feedbacks. At the annual scale, the more pronounced warming rate of winters (figs. S2 and S3)—due to anthropogenic background warming—overwhelms the land-atmosphere feedback effects that are activated in the warm season. Nevertheless, increasing temperature trends increases the probability of concurrence of dry and hot extremes.

Temporal trends in compound dry-hot extremes

We use return period as a statistical measure of the severity and likelihood of an extreme event. Return period signifies the expected recurrence of a phenomenon (*25*); for example, a 25-year event is expected to occur, on average, once in 25 years, which is associated with an exceedance probability of 0.04 (nonexceedance probability of 0.96). This definition is intuitive for univariate extremes, such as dryness. However, the concept is rather complex for multivariate cases (*20*). Here, we use the AND hazard scenario, which determines the probability (or frequency) of a compound dry-hot event, i.e., drier than a threshold AND hotter than a threshold (*26*). We use the empirical copula and the entire 122 years of the record to estimate the joint exceedance probabilities of dryness and heat excess. We focus on the annual precipitation and mean annual temperature in this paper. The results for annual precipitation and mean spring-summer temperature, as well as spring-summer precipitation and mean spring-summer temperature, are provided in the Supplementary Materials (figs. S14 to S17). Mean annual temperature is selected here to include winter temperature, which, along with spring, is warming at a higher rate compared to other seasons (*27*). Winter temperature has important environmental implications ranging from snowmelt and water availability to phenology and wildlife health. Mean annual temperature is also closely associated with soil respiration that has important feedbacks with climate. Moreover, an increase in mean annual temperature is associated with a pronounced likelihood of extreme heat events (*28*).

The frequency of >25-year compound dry-hot extremes (joint return period levels exceeding 25 years) has significantly increased

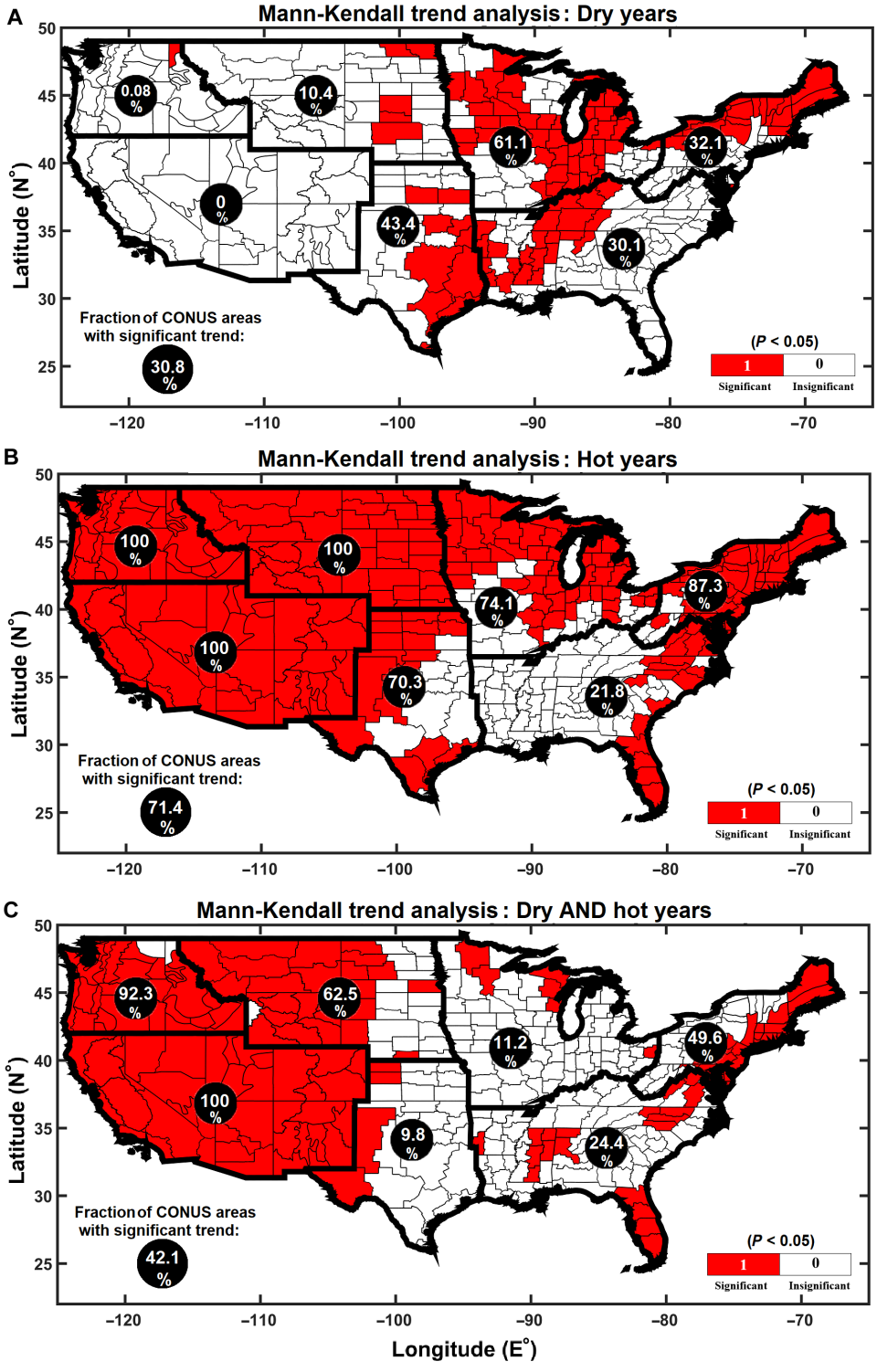

Fig. 1. Nonparametric Mann-Kendall trend analysis. Red shaded areas show a statistically significant increase (at the 5% level) in the return period level of (**A**) dry extremes, (**B**) hot extremes, and (**C**) concurrent dry AND hot extremes across CONUS over the past 122 years (1896–2017) at the annual scale. Fraction of area in each region and the entire CONUS with significant trends are also shown in the figure.

over the last three quarter-century periods (Fig. 2, A to C). While in 1943–1967 most of the climate divisions across CONUS observed only one >25-year compound dry-hot extreme (as expected per the definition of such an event), with some climate divisions not observing any, this increased slightly to one to three such bivariate events in 1968–1992 for almost all climate divisions in CONUS. In the most recent period (1993–2017), however, there is a spike in the number of >25-year compound dry-hot extremes, with several

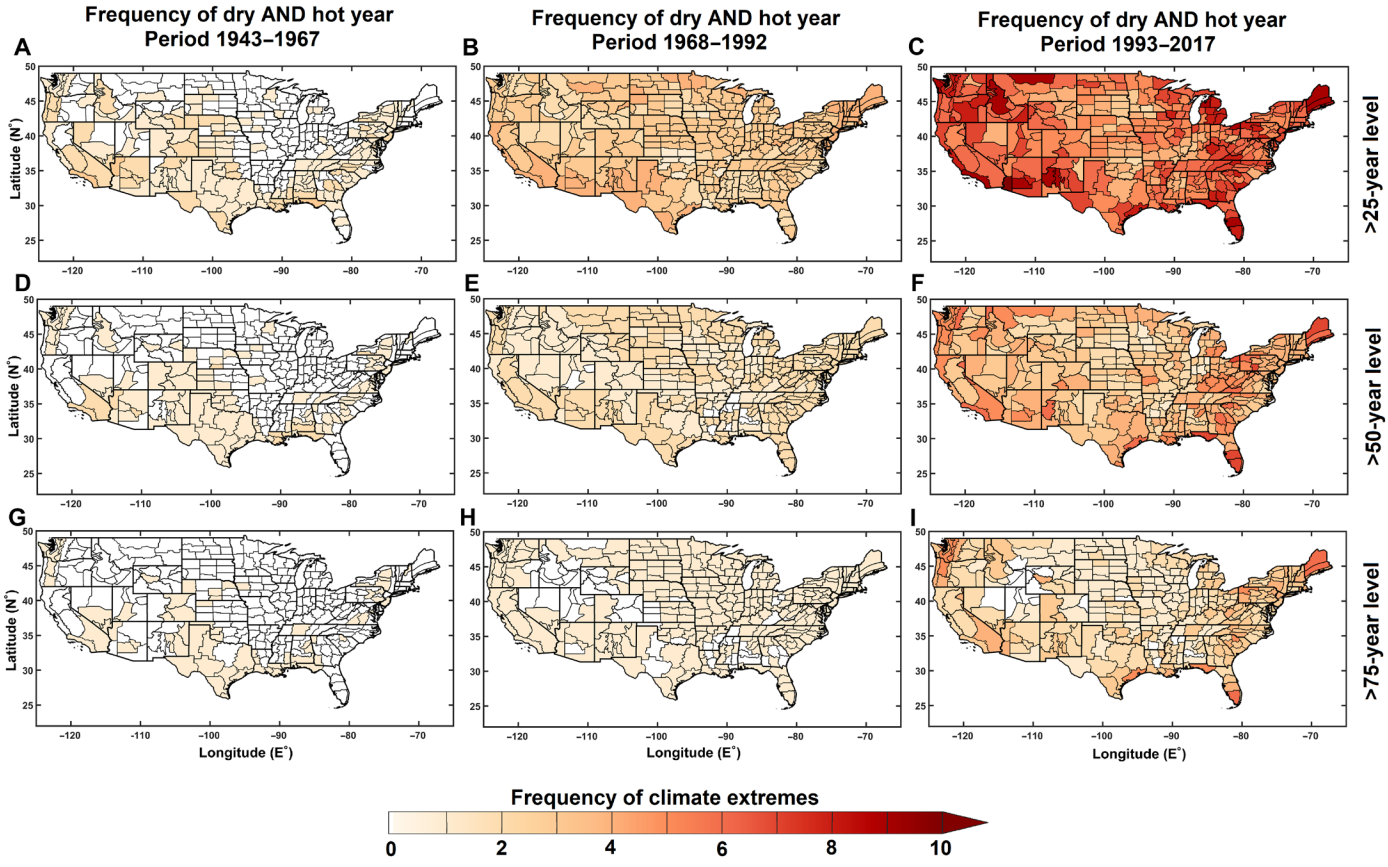

Fig. 2. Frequency of compound dry-hot extremes has increased. (**A** to **C**) Frequency of >25-year, (**D** to **F**) frequency of >50-year, and (**G** to **I**) frequency of >75-year bivariate dry AND hot extremes across CONUS in the periods of 1943–1967 (A, D, and G), 1968–1992 (B, E, and H), and 1993–2017 (C, F, and I).

climate divisions observing more than five such compound events. The increase is most pronounced for the Pacific Northwest, southern portions of the Southwest, Florida, and portions of the Northeast. This escalation in the frequency of compound dry-hot extremes extends beyond the expected randomness of climate phenomena. The nonparametric Mann-Kendall trend analysis of the return period level of compound events over the past 122 years shows a statistically significant trend at the 5% level for the western CONUS, Florida, the eastern portion of the Northeast, and some climate divisions in Michigan, Minnesota, Mississippi, and Alabama (Fig. 1C). Similar inferences about more frequent compound dry-hot extremes could be made for >50-year (Fig. 2, D to F) and >75-year (Fig. 2, G to I) events. Multiple >75-year compound events are observed in the coastal Pacific Northwest, inland Southern California, Florida, Maine, and several climate divisions in Texas, which point to the intensification of compound dry-hot extremes over many portions of CONUS with significant socio-environmental repercussions, such as causing very large wildfires (*29*).

These results are in accordance with the findings of Hao *et al.* (*19*) and Mazdiyasni and Kouchak (*14*) that show an increasing frequency of concurrence of precipitation and temperature extremes over the globe and CONUS, respectively. The spatial distribution of compound extremes in our study, however, is not in complete agreement with that of Mazdiyasni and Kouchak (*14*) (Fig. 1), especially for California and the Pacific Northwest. This discrepancy stems from differences in the definitions of compound events, along with differences in the study period. Here, we define the compound events as years with <0.04 exceedance probability of being dry AND hot (>25-year return level), whereas they use meteorological drought and various definitions of heatwaves as compound events. Moreover, their study spans 1960–2010, whereas our study spans 1896–2017. This longer time period can add significant information on the frequency of compound dry-hot extremes, as it includes the megadrought of the 1930s (discussed in the next section).

Spatial trends in compound dry-hot extremes

Our analysis points to a substantial increase in the number of climate divisions observing >25-year compound dry-hot extremes after the 1950s across all climate regions in the CONUS (Fig. 3, A to G). This increasing trend, however, is not present for many regions if one uses a longer record (1896–2017). More specifically, there is no increasing trend observed in the number of climate divisions observing >25-year compound dry-hot extremes for the Great Plains, Midwest, and Southeast, and to some extent the Northeast (Fig. 3, A to G). However, there is an interesting shift in the nature of the dominant driver for these compound events. In the 1930s, a long, severe dry event that engulfed two-thirds of CONUS was the dominant driver of the joint probability of compound dry-hot extremes. This drought contributed to the infamous dust storms of the Southern Great Plains (*30*). In the mid-2000s, however, both precipitation deficit and heat excess contributed to the compound events across many climate regions (Fig. 3, A, B, and G), and since 2010, hotter years

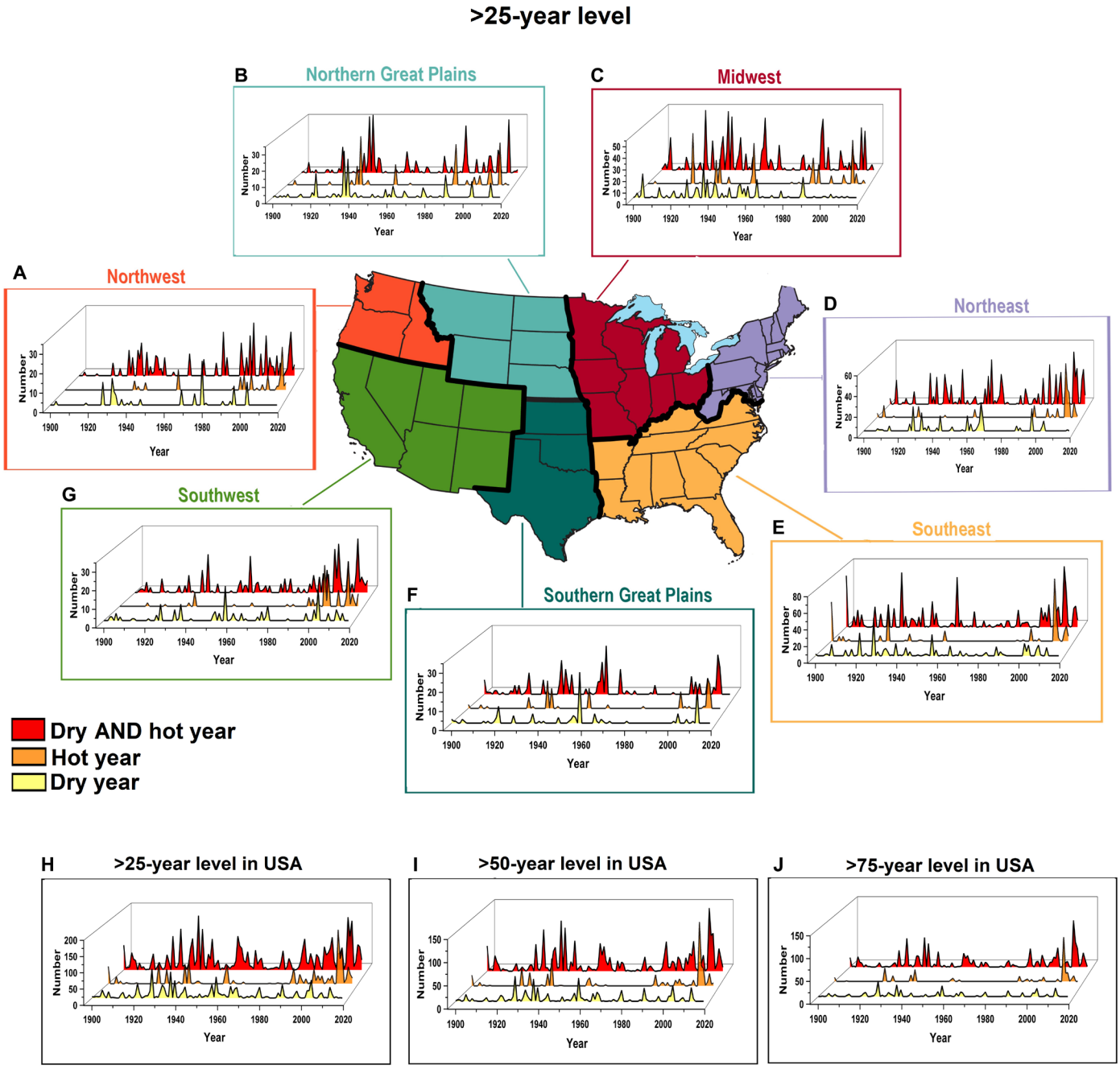

Fig. 3. Number of climate divisions affected by compound dry-hot extremes is increasing across many regions. (**A** to **G**) Different regions of CONUS affected by >25-year univariate dry, univariate hot, and bivariate dry AND hot extremes. (**H** to **J**) Entire CONUS affected by >25-year, >50-year, and >75-year extremes, between 1896 and 2017.

became the main driver of the compound events across all the climate regions (Fig. 3, A to G). This observation is in accordance with the findings of Mo and Lettenmaier (*24*), who reported that heatwave-driven flash droughts have shown an increasing trend across CONUS since 2011. This implies that the dominant triggering driver of the land-atmosphere feedback has shifted from dryness in the earlier half of the study to excess heat in recent decade(s).

Over the entire CONUS, the number of climate divisions with >25-, >50-, and >75-year compound dry-hot extremes shows an increasing trend, with >75-year events having the highest rate of increase (i.e., a larger slope of linear regression; Fig. 3, H to J). These results also confirm the shift in the main driver of the compound extreme events from dry years in the 1930s to hot years in recent decade(s). Many compound event studies focus on the concurrence of droughts and heatwaves, and, in general terms, dry and hot years, over the past 3 to 6 decades (*15*, *19*, *31*). Climate analysis studies should use longer time series to also detect low-frequency cycles of the climate (*32*). We argue that the literature might underestimate the risks of compound dry-hot extremes by neglecting to account for longer climatic cycles and lower frequency events, such as the

1930s drought. Lower-frequency cycles of climate are most likely to bring back historical multidecadal and continental megadroughts in the United States (*32*–*34*). While internal stochastic—not forced—atmospheric variability alone is able to create both megadroughts (*35*) and megaheatwaves (*36*), anthropogenic emissions have considerably increased their probability of occurrence (*37*) and, most importantly, their concurrence (*13*).

The cumulative area (km^2) affected by >25-year compound dry-hot years also shows a statistically significant increasing trend at the 10% level as determined by the nonparametric Mann-Kendall trend analysis (Fig. 4). The highest increase rate (slope of the linear regression of cumulative impacted area as a function of time) is associated with the Southeast, Northeast, and Southwest, respectively. This, however, does not account for the total area of each climate region, and care is advised in interpreting these results for comparison purposes. Furthermore, the area affected by >25-year hot years is also associated with an increasing trend across all climate regions, which is determined to be nonsignificant at the 10% level. The cumulative area observing >25-year dry years, however, is not associated with an increasing or a decreasing trend.

Further analysis shows that the cumulative distribution of the percent of CONUS observing >25-year compound dry-hot years for 1993–2017 (the past 25-year period) diverges from that of 1896–1920 (the first 25-year period; fig. S8C). This divergence is also visible for >25-year hot years (fig. S8B) but is less marked for >25-year dry years (fig. S8A) between the periods of 1896–1920 and 1993–2017. Moreover, the Kolmogorov-Smirnov, Cramér-von Mises, and Anderson-Darling tests all point to statistically significant shifts in the cumulative distributions of the percent of CONUS observing >25-year compound dry-hot and univariate hot years between 1993 and 2017 and 1896 and 1920, which correspond to the last and the first 25-year periods of our study (table S1). This distribution for >25-year dry years, however, is not statistically different between the two periods

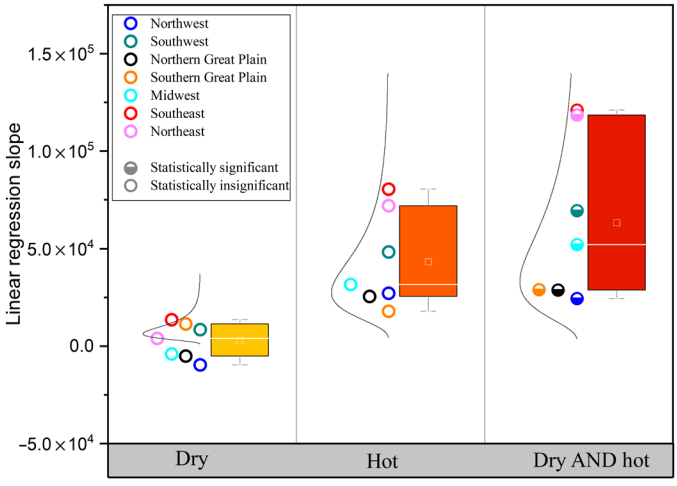

Fig. 4. Impacted areas by >25-year compound dry-hot extremes are enlarging. Slope of linear regression to the spatial extent of >25-year univariate dry, univariate hot, and bivariate dry AND hot extremes based on the affected area size (km^2). Filled circles are associated with statistically significant trends at the 10% level, and empty circles are associated with trends that are not statistically significant at the 10% level. None of the increases are significant at the 5% level. Boxes represent the range between the 25th and 75th percentiles of the linear regression slopes, and the horizontal line in each box corresponds to the slopes' median.

at the 5% (and the 10%) level using the Kolmogorov-Smirnov and Cramér-von Mises tests, although the Anderson-Darling test points to their significant divergence (table S1). We repeated these tests for different 25-year periods compared to 1993–2017; results generally point to significant changes in cumulative distribution of the percent of CONUS affected by >25-year compound dry-hot extremes (except for the 1918–1942 period) and >25-year hot years, but generally do not identify significant changes in distributions of >25-year dry years (table S2). Rather, similar results are observed if the two periods of 1896–1956 and 1957–2017 are used (61-year periods; table S3).

Spatial homogeneity of compound dry-hot extremes

It is also important to analyze homogeneity of the area affected by compound dry-hot extremes. Large spatially homogenous compound events can endanger natural and built system services (*38*). For natural systems, connected heterogeneous habitats are resilient to synchronous and large-scale aquatic species population and ecosystem collapse. Homogeneous compound dry-hot events might fragment this connectedness and result in population collapse. In the context of built systems, homogeneous compound extremes can damage harvests across a wide range of agricultural lands and rapidly deplete federal and local relief resources.

Here, we assess the connectedness of climate divisions that experience >25-year compound dry-hot extremes. We calculate the spatial correlation in terms of impacted area (km^2) through Moran's I as a proxy for spatial homogeneity for compound dry-hot, as well as univariate dry and univariate hot extremes for each year (fig. S9). We show that spatial homogeneity of >25-year dry years is associated with a nominal slope that fluctuates between negligible negative and positive values for different climate regions as well as the entire CONUS over the past 122 years (Fig. 5). The spatial homogeneity of >25-year hot years shows an increasing trend with linear slopes of Moran's I ranging between 0.04 and 0.07 across various regions (Fig. 5). Similarly, >25-year compound dry-hot extremes are also growing homogeneously with a slope of linear regression of Moran's I ranging from 0.1 to 0.18 across different regions. Homogeneous enlargement of compound events is steeper than each of the drivers alone, with the largest difference observed in the Southwest (0.18 versus 0.02). To investigate the potential impact of the threshold of extreme events (>25-year) on the observed connectivity trend (*39*), Moran's I analysis was performed on less (>5-year) and more (75-year) intense extreme events (figs. S10 and S11), the results of which confirm those found for the >25-year analysis. Further, the cumulative distribution of annual Moran's I for >25-year compound dry-hot years between 1896 and 1956, and 1957 and 2017, is determined to be statistically different based on the Kolmogorov-Smirnov, Cramér-von Mises, and Anderson-Darling tests at the 5% level (table S4). These tests are also applied to the distributions of Moran's I for various 25-year periods (table S5).

If the past 50 years alone are analyzed, the homogeneous spatial growth of >25-year compound dry-hot years shows an even steeper slope, mainly driven by the homogeneous enlargement of hot years (fig. S12). The slope of Moran's I for compound extremes ranges between 0.1 and 0.6 for various regions and is 0.7 for the entire CONUS. This ranges between 0.1 and 0.4 for different regions and 0.6 for the entire CONUS for >25-year hot years. Conversely, dry years do not exhibit much change in terms of spatial homogeneity. In this period, while the growth rate (slope of linear regression to Moran's I)

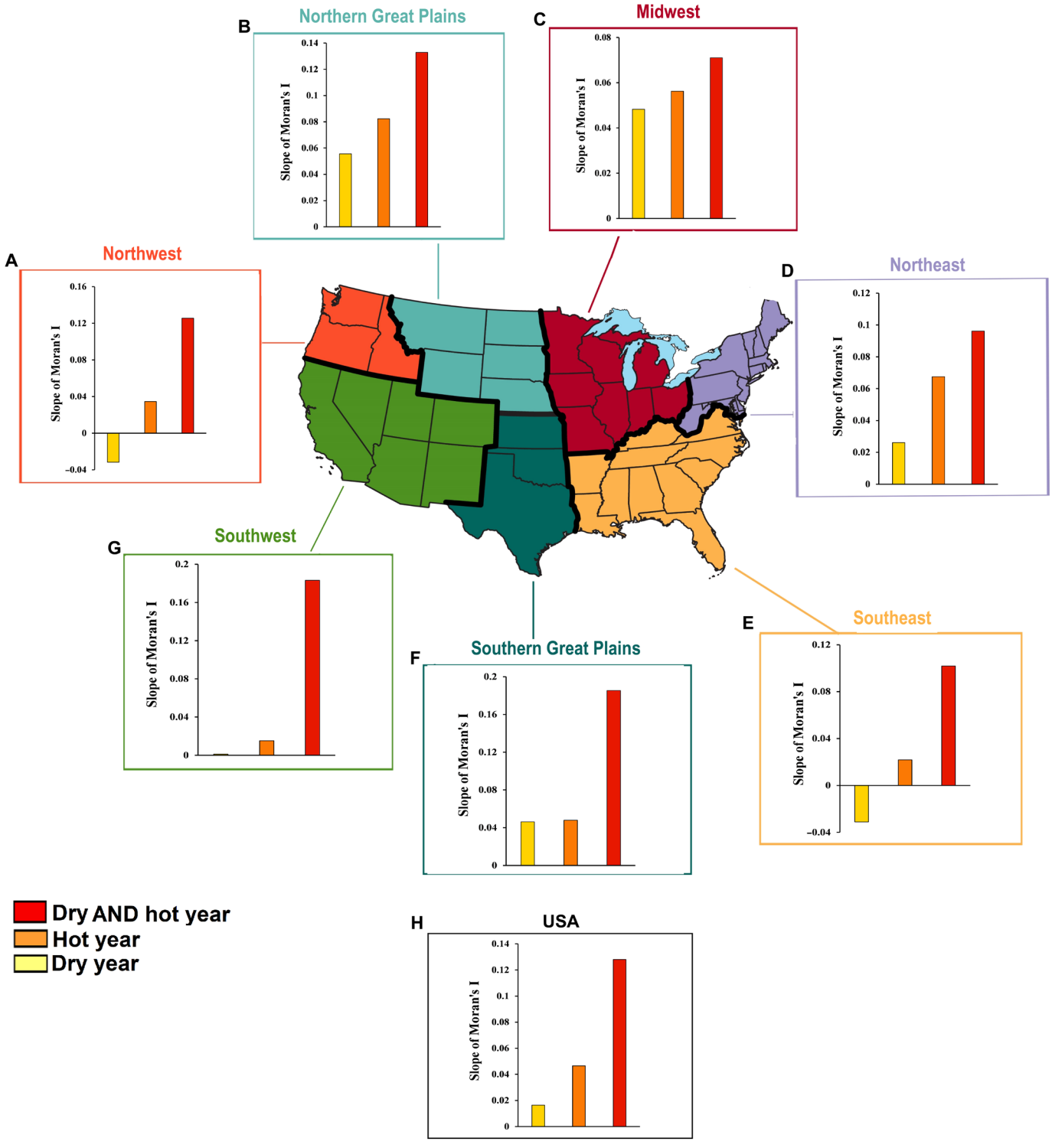

Fig. 5. Spatial homogeneity for compound dry-hot extremes is increasing. Slope of linear regression to time series of Moran's I of >25-year univariate dry, univariate hot, and bivariate dry AND hot extremes for different climate regions (**A** to **G**) as well as the entire CONUS (**H**) over the past 122 years (1896–2017).

for the compound events and the univariate hot extremes for the Northwest, Northern Great Plains, and Midwest are rather similar (slightly higher for compound events), the increase in homogeneity of compound events over the rest of CONUS occurs at a much higher rate than the increase in univariate hot extremes.

DISCUSSION

Persistent large-scale circulation anomalies are generally known to initiate drought and heatwave events and their co-occurrence; however, land-atmosphere feedbacks can also intensify and propagate those anomalous climatic events (*40*). Megaheatwaves, for example,

are usually preceded by persistent anticyclones, enabling cloud-free conditions and advection of hot air (*40*), but drier soils intensify heatwaves by partitioning the incoming solar radiation into more sensible and less latent heat. It is noted that megaheatwaves can be generated by natural atmospheric variability even without land-atmosphere feedbacks (*36*). However, land-atmosphere feedbacks increase the probability of occurrence of megaheatwaves (*41*). For example, the probability of the Russian 2010 megaheatwave event increased 13-fold due to the self-intensification feedback of drought and heatwave (*42*). With a lack of soil moisture, evaporation decreases as does partitioning of solar radiation into latent heat; hence, a larger fraction of the incoming radiation is translated into sensible heat, which, in turn, warms the environment (*43*). Desiccated soils contribute to temperature increase, heat entrainment, and deepening of the atmospheric boundary layer. The latter, in turn, increases evaporative demand and further desiccates soils and further increases the temperature. This cycle of drying and warming inhibits the formation of clouds and, in turn, restrains local convective precipitation, further intensifying drought (*40*).

A less explored mechanism of land-atmosphere feedback is self-propagation (*40*). In a Lagrangian perspective, atmospheric moisture deficit and heat can propagate from one location to downwind regions (*18*). While heat advection and its impact on the formation and expansion of heatwaves have been explored in the literature, especially for the 2003 European and 2010 Russian megaheatwaves (*44*), terrestrially sourced atmospheric moisture advection has been explored in less detail but is receiving more attention in the recent literature (*18*). Within-continent transport of terrestrially sourced moisture has promoted the concept of "teleconnected land-atmosphere feedbacks" (*10*). While this concept is still in its infancy, these teleconnected land-atmosphere feedbacks are believed to help propagate droughts to neighboring regions (*10*, *18*). The propagation of droughts is more important for regions that depend on terrestrially sourced precipitation, including large parts of North America (*45*). Our analysis shows that compound dry-hot extremes have enlarged homogeneously, i.e., impacted areas are increasingly becoming connected, pointing to the propagation of atmospheric moisture deficit AND heat from one region to its neighboring regions. Connected spatial growth of compound dry-hot events can have significant natural and societal repercussions. An example of a spatially large and severe compound extreme is the summer 2010 drought and heatwave in Russia that decreased crop production by 25%, caused >500 wildfires that burned more than 1 million ha, and induced an estimated 15 billion USD economic loss (*46*).

Our results show that the frequency of compound dry-hot extremes in CONUS has substantially increased in the past 50 years, a trend that is less pronounced if a longer period of analysis (1896–2017) is used. While anomalous synoptic circulation patterns are recognized for initiation of compound dry-hot events, background warming due to anthropogenic emissions has strengthened, caused the earlier start of, and extended the spatial impact of land-atmosphere feedbacks in North America (*12*). We report that there is a shift in the dominant driver of compound dry-hot extremes from precipitation deficit in the 1930s to heat excess in recent decade(s). In other words, the dominant driver that triggers land-atmosphere feedbacks has changed from meteorological drought to excess heat. This is in concept similar to the precipitation deficit–driven and heatwave-driven flash drought categorization of Mo and Lettenmaier (*24*, *47*), despite differences in the temporal scale. Although flash droughts of all categories are shown to have increased in frequency across the globe in the last century, Mo and Lettenmaier (*24*) show that the frequency of heatwave-driven flash droughts was associated with a decreasing trend over the last century, which rebounded after 2011. This agrees with our argument of the changing nature of the dominant driver of compound dry-hot events in the recent decade, i.e., precipitation deficit to heat excess. Further, while natural variability is able to create compound events, anthropogenic emissions have significantly enhanced the probability of concurrent drought and heatwaves, and only aggressive emission reduction can mitigate the risks associated with their increasing frequency (*13*). Last, although notable variations exist over different regions of CONUS, there is no significant increasing trend in the frequency of univariate dry years; however, univariate hot years are becoming more frequent and more intense.

We argue that recent literature may underestimate the risks of concurrent dry and hot episodes, as they only study the post-1950s period without recourse to the 1930s meteorological drought that engulfed two-thirds of CONUS for almost a decade. We argue that if meteorological droughts of the length and severity observed in the 1930s occur during the hot years that are increasingly common in recent decades due to global warming, their concurrence can have devastating impacts (*5*, *32*, *48*). Recent literature shows that no major U.S. region is immune to the multidecadal continental-scale megadroughts that occurred in the 12th and 13th centuries (*49*), and global warming has markedly increased the risk of their return (*37*). Moreover, a hotter climate increases water demand (*50*), concurrence of which with dry years would strain social, built, and natural systems (*7*) and might push them to unprecedented states (*51*). Our results contribute to a deeper understanding of the spatiotemporal patterns of compound events to help with reliable risk projections in the context of climate change. The consequences of the increased frequency, intensity, and spatial homogeneity of climatic extremes for compound events with multiple drivers are far graver than the effect of each driver individually (*9*), and risk assessment frameworks need to consider the compounding effects of multiple extremes rather than addressing one driver at a time within the traditional univariate framework.

MATERIALS AND METHODS

Compound dry and hot events versus drought

As defined by the Intergovernmental Panel on Climate Change (IPCC) Special Report on Managing the Risks of Extreme Events and Disasters to Advance Climate Change Adaptation (SREX) report, drought is the "impact of extreme weather or climate events on the natural physical environment." Drought is a complex phenomenon with multiple drivers, the most complicated of which are human activities that regulate and affect input, output, and shortage of water in the human-environment system. Human influences can modify and regulate drought and even cause drought in the absence of its natural drivers (*52*). In this paper, we are interested in the extremes that cause drought, i.e., compound dry and hot events.

Joint probabilities and return periods

The joint probability and bivariate return periods of extreme events are calculated on the basis of the empirical copula models using the AND scenario. Copulas are statistical measures that explore the dependence and association between two or more variables regardless of their univariate distributions and provide a multivariate distribution (*53*). A bivariate copula can be informally defined as mapping

from $I^2(F, G) \rightarrow I(H)$, where $(F(x), G(y), H(x, y))$ is a point from I^3, ($I \in [0,1]$). X and Y are continuous random variables with distribution functions $F(x) = P(X \leq x)$, $G(y) = P(Y \leq y)$, and $H(x, y) = P(X \leq x, Y \leq y)$ is a function that describes their joint distribution. Let H be a joint cumulative distribution function with marginal univariate distributions F and G. Then, there exists a copula C so that $H(x, y) = C[F(x), G(y)]$. Considering the joint distribution H with continuous marginals F and G, $u = F(x)$, $v = G(y)$, the associated copula can be described as

$$C(u,v) = H\left[F^{-1}(u), G^{-1}(v)\right] \tag{1}$$

The bivariate joint exceedance probability in terms of the AND scenario can be defined as

$$P(X > x \wedge Y > y) = 1 - F(x) - G(y) + C\left[F(x), G(y)\right] \tag{2}$$

and the associated return period, RP, based on the AND scenario is defined as

$$\mathrm{RP}_{\mathrm{AND}} = \frac{1}{P(X > x \wedge Y > y)} \tag{3}$$

We adopt a nonparametric approach to calculate univariate and multivariate probabilities and associated return periods. This relaxes the need for fitting parametric distributions to data, which are associated with underlying assumptions. Violation of assumptions can produce biased and unreliable results. Further, one parametric model may not be appropriate for all climate divisions across CONUS, which poses grave challenges on spatial comparison of results. Nonparametric approaches, on the contrary, are accurate and do not depend on any underlying assumption.

Spatial autocorrelation

The spatial autocorrelation of compound extreme events over a time period is determined using Moran's I (*54*, *55*), which is a cross-product statistic between a variable and its spatial lag. For an observation at the location i, the deviation of observation from its mean (z_i) is expressed as $z_i = x - \hat{X}$, where $\hat{X}$ is the mean of variable x. Moran's I statistic for spatial autocorrelation is given as

$$I = \frac{\Sigma_i \Sigma_j w_{i,j} z_i . z_j / S_0}{\Sigma_i {z_i}^2 / n} \tag{4}$$

where $w_{i,j}$ is the element i, j of the spatial weights' matrix, n is the number of observations, and S_0 is the aggregate of all the spatial weights: $S_0 = \Sigma_i \Sigma_j w_{i,j}$. Spatial autocorrelation has a value between −1 and 1. Positive and negative values signify spatial clustering of similar and dissimilar values, respectively (1: perfect clustering, and −1: perfect dispersion), and a zero value specifies absence of spatial autocorrelation (perfect randomness) (*56*).

Temporal trends

Mann-Kendall trend test (*57*, *58*) is a nonparametric test commonly used to statistically assess whether there is a monotonic trend in the time series of the variable of interest. The null hypothesis, H_0, states that that there is no monotonic trend in the series, and the data come from a population with independent realizations and are identically distributed. The alternative hypothesis, H_1, is that a trend exists and the data follow a monotonic trend (positive or negative).

For a given time series $(x_1, \ldots, x_n)$, the sign of all $n(n-1)/2$ possible differences $(x_j - x_i)$, $j > i$ is determined. Using the indicator function S, the number of discrepancies between positive and negative signs is computed as follows

$$S = \sum_{i=1}^{n-1} \sum_{j=k+1}^{n} \mathrm{sign}(x_j - x_i) \tag{5}$$

If $S > 0$, later observations in the time series tend to be larger than observations made earlier, and the reverse is true if $S < 0$.

The variance of S is presented by

$$\mathrm{Var}(s) = \frac{1}{18}\left[n(n-1)(2n+5) - \sum_p t_p(t_p - 1)(2t_p + 5)\right] \tag{6}$$

where t_p is the frequency of times that the rank t emerges. p differs over the set of the tied groups.

The Mann-Kendall trend analysis calculates the test statistic Z_{MK} as follows

$$Z_{\mathrm{MK}} = \begin{cases} \frac{S-1}{\sqrt{\mathrm{Var}(S)}} & \text{if } S > 0 \\ 0 & \text{if } S = 0 \\ \frac{S+1}{\sqrt{\mathrm{Var}(S)}} & \text{if } S < 0 \end{cases} \tag{7}$$

A positive/negative value of Z_{MK} shows a positive/negative trend in the time series with time.

Distribution tests

The two-sample Cramér-von Mises test and Anderson-Darling test are commonly used to assess changes in probability distributions, and both tests refer to the class of empirical distribution function (EDF). The null hypothesis, H_0, for these tests is that the data come from the same distribution. Considering F_m and F_n as empirical distributions of the two samples, the Cramér-von Mises test statistic proceeds by computing the distance between F_m and F_n distributions as

$$\mathrm{CM} = \int_{-\infty}^{+\infty} |F_n(x) - F_m(x)|^2 \, \mathrm{dF}(x) \tag{8}$$

The two-sample Anderson-Darling statistic test is presented by (*59*)

$$A^2 = \frac{mn}{t} \int_{-\infty}^{+\infty} \frac{[F_n(x) - F_m(x)]^2}{H_t(x)[1 - H_t(x)]} dH_t(x) \tag{9}$$

where $t = m + n$, and $H_t(x) = \frac{[nF_n(x) + mF_m(x)]}{t}$ is the EDF of the combined sample.

The judgment to reject the null hypothesis (H_0) depends on comparing the value of test statistics for the hypothesis test and the specified significance level. If the value of the test statistic is greater than the significance level ($P = 0.05$), the null hypothesis will be rejected.

Similarly, the Kolmogorov-Smirnov test measures the distance between the EDF of F_m and F_n as the empirical distributions. The test statistic is specified by (*60*)

$$D_n = \sup_x |F_n(x) - F_m(x)| \tag{10}$$

where $\sup_x$ is the supremum of the set of distances. The null hypothesis, H_0, is rejected if D_n is greater than the significance level ($P = 0.05$).

Climate divisions

Climate Divisional Dataset provides a complete set of long-term spatiotemporal data for historical climate analyses over CONUS. There are 344 climate divisions in CONUS, in which monthly temperature and precipitation are estimated using daily observations. The complete list of climatological divisions can be found at https://ncdc.noaa.gov/monitoring-references/maps/us-climate-divisions.php.

Climate region

CONUS is grouped into seven similar climatological regions including the Northeast, Southeast, Northwest, the Southwest, the Northern Great Plains, Southern Great Plains, and the Midwest, which provide greater detail and information regarding national climate assessments.

SUPPLEMENTARY MATERIALS

Supplementary material for this article is available at http://advances.sciencemag.org/cgi/content/full/6/39/eaaz4571/DC1

REFERENCES AND NOTES

1. J. Zscheischler, S. I. Seneviratne, Dependence of drivers affects risks associated with compound events. *Sci. Adv.* **3**, e1700263 (2017).
2. C. Schär, P. L. Vidale, D. Lüthi, C. Frei, C. Häberli, M. A. Liniger, C. Appenzeller, The role of increasing temperature variability in European summer heatwaves. *Nature* **427**, 332–336 (2004).
3. J. Hansen, R. Ruedy, M. Sato, K. Lo, Global surface temperature change. *Rev. Geophys.* **48**, RG4004 (2010).
4. A. Dai, Characteristics and trends in various forms of the Palmer Drought Severity Index during 1900–2008. *J. Geophys. Res. Atmos.* **116**, D12115 (2011).
5. B. Mueller, S. I. Seneviratne, Hot days induced by precipitation deficits at the global scale. *Proc. Natl. Acad. Sci. U.S.A.* **109**, 12398–12403 (2012).
6. M. Leonard, S. Westra, A. Phatak, M. Lambert, B. van den Hurk, K. M. Innes, J. Risbey, S. Schuster, D. Jakob, M. Stafford-Smith, A compound event framework for understanding extreme impacts. *Wiley Interdiscip. Rev. Clim. Change* **5**, 113–128 (2014).
7. A. P. Williams, C. D. Allen, A. K. Macalady, D. Griffin, C. A. Woodhouse, D. M. Meko, T. W. Swetnam, S. A. Rauscher, R. Seager, H. D. Grissino-Mayer, J. S. Dean, E. R. Cook, C. Gangodagamage, M. Cai, N. G. McDowell, Temperature as a potent driver of regional forest drought stress and tree mortality. *Nat. Clim. Chang.* **3**, 292–297 (2013).
8. S. B. Guerreiro, R. J. Dawson, C. Kilsby, E. Lewis, A. Ford, Future heat-waves, droughts and floods in 571 European cities. *Environ. Res. Lett.* **13**, (2018).
9. J. Zscheischler, S. Westra, B. J. J. M. van den Hurk, S. I. Seneviratne, P. J. Ward, A. Pitman, A. A. Kouchak, D. N. Bresch, M. Leonard, T. Wahl, X. Zhang, Future climate risk from compound events. *Nat. Clim. Change* **8**, 469–477 (2018).
10. D. G. Miralles, P. Gentine, S. I. Seneviratne, A. J. Teuling, Land–atmospheric feedbacks during droughts and heatwaves: State of the science and current challenges. *Ann. N. Y. Acad. Sci.* **1436**, 19–35 (2019).
11. A. A. Kouchak, L. Cheng, O. Mazdiyasni, A. Farahmand, Global warming and changes in risk of concurrent climate extremes: Insights from the 2014 California drought. *Geophys. Res. Lett.* **41**, 8847–8852 (2014).
12. P. A. Dirmeyer, Y. Jin, B. Singh, X. Yan, Evolving land–atmosphere interactions over North America from CMIP5 simulations. *J. Climate* **26**, 7313–7327 (2013).
13. A. Sarhadi, M. C. Ausín, M. P. Wiper, D. Touma, N. S. Diffenbaugh, Multidimensional risk in a nonstationary climate: Joint probability of increasingly severe warm and dry conditions. *Sci. Adv.* **4**, eaau3487 (2018).
14. O. Mazdiyasni, A. A. Kouchak, Substantial increase in concurrent droughts and heatwaves in the United States. *Proc. Natl. Acad. Sci. U.S.A.* **112**, 11484–11489 (2015).
15. S. Sharma, P. Mujumdar, Increasing frequency and spatial extent of concurrent meteorological droughts and heatwaves in India. *Sci. Rep.* **7**, 15582 (2017).
16. F. Chiang, O. Mazdiyasni, A. A. Kouchak, Amplified warming of droughts in southern United States in observations and model simulations. *Sci. Adv.* **4**, eaat2380 (2018).
17. D. G. Miralles, D. Schumacher, J. Keune, C. van Heerwaarden, Jordi Vilà-Guerau de Arellano, P. Gentine, S. I. Seneviratne, A. Teuling, Mega-heatwave temperatures driven by local and upwind soil desiccation. *Geophys. Res. Abstr.* **1** (2019).
18. J. E. Herrera-Estrada, J. A. Martinez, F. Dominguez, K. L. Findell, E. F. Wood, J. Sheffield, Reduced moisture transport linked to drought propagation across North America. *Geophys. Res. Lett.* **46**, 5243–5253 (2019).
19. Z. Hao, A. A. Kouchak, T. J. Phillips, Changes in concurrent monthly precipitation and temperature extremes. *Environ. Res. Lett.* **8**, 034014 (2013).
20. S. Corbella, D. D. Stretch, Multivariate return periods of sea storms for coastal erosion risk assessment. *Nat. Hazards Earth Syst. Sci.* **12**, 2699–2708 (2012).
21. C. B. Field, V. R. Barros, D. J. Dokken, K. J. Mach, M. D. Mastrandrea, T. E. Bilir, M. Chatterjee, K. L. Ebi, Y. O. Estrada, R. C. Genova, B. Girma, E. S. Kissel, A. N. Levy, S. MacCracken, P. R. Mastrandrea, L. L. White, Eds., *Climate Change 2014—Impacts, Adaptation and Vulnerability: Regional Aspects* (Cambridge Univ. Press, 2014).
22. M. Bayazit, B. Önöz, To prewhiten or not to prewhiten in trend analysis? *Hydrol. Sci. J.* **52**, 611–624 (2007).
23. M. Hoerling, J. Eischeid, A. Kumar, R. Leung, A. Mariotti, K. Mo, S. Schubert, R. Seager, Causes and predictability of the 2012 great plains drought. *Bull. Am. Meteorol. Soc.* **95**, 269–282 (2014).
24. K. C. Mo, D. P. Lettenmaier, Heat wave flash droughts in decline. *Geophys. Res. Lett.* **42**, 2823–2829 (2015).
25. M. Sadegh, H. Moftakhari, H. V. Gupta, E. Ragno, O. Mazdiyasni, B. Sanders, R. Matthew, A. A. Kouchak, Multihazard scenarios for analysis of compound extreme events. *Geophys. Res. Lett.* **45**, 5470–5480 (2018).
26. B. Gräler, M. J. van den Berg, S. Vandenberghe, A. Petroselli, S. Grimaldi, B. De Baets, N. E. C. Verhoest, Multivariate return periods in hydrology: A critical and practical review focusing on synthetic design hydrograph estimation. *Hydrol. Earth Syst. Sci.* **17**, 1281–1296 (2013).
27. J. M. Melillo, T. Richmond, G. W. Yohe, *Climate Change Impacts in the United States: The Third National Climate Assessment* (U.S. Global Change Research Program, 2014).
28. N. S. Diffenbaugh, D. Singh, J. S. Mankin, D. E. Horton, D. L. Swain, D. Touma, A. Charland, Y. Liu, M. Haugen, M. Tsiang, B. Rajaratnam, Quantifying the influence of global warming on unprecedented extreme climate events. *Proc. Natl. Acad. Sci. U.S.A.* **114**, 4881–4886 (2017).
29. J. T. Abatzoglou, A. P. Williams, Impact of anthropogenic climate change on wildfire across western US forests. *Proc. Natl. Acad. Sci. U.S.A.* **113**, 11770–11775 (2016).
30. S. D. Schubert, M. J. Suarez, P. J. Pegion, R. D. Koster, J. T. Bacmeister, On the cause of the 1930s dust bowl. *Science* **303**, 1855–1859 (2004).
31. D. L. Swain, D. E. Horton, D. Singh, N. S. Diffenbaugh, Trends in atmospheric patterns conducive to seasonal precipitation and temperature extremes in California. *Sci. Adv.* **2**, e1501344 (2016).
32. J. T. Overpeck, Climate science: The challenge of hot drought. *Nature* **503**, 350–351 (2013).
33. B. I. Cook, R. L. Miller, R. Seager, Amplification of the north american "Dust Bowl" drought through human-induced land degradation. *Proc. Natl. Acad. Sci. U.S.A.* **106**, 4997–5001 (2009).
34. R. Seager, Y. Kushnir, C. Herweijer, N. Naik, J. Velez, Modeling of tropical forcing of persistent droughts and pluvials over Western North America: 1856–2000. *J. Climate* **18**, 4065–4088 (2005).
35. B. I. Cook, E. R. Cook, J. E. Smerdon, R. Seager, A. P. Williams, S. Coats, D. W. Stahle, J. V. Díaz, North American megadroughts in the Common Era: Reconstructions and simulations. *Wiley Interdiscip. Rev. Clim. Chang.* **7**, 411–432 (2016).
36. R. Dole, M. Hoerling, J. Perlwitz, J. Eischeid, P. Pegion, T. Zhang, X.-W. Quan, T. Xu, D. Murray, Was there a basis for anticipating the 2010 Russian heat wave? *Geophys. Res. Lett.* **38**, L06702 (2011).
37. N. J. Steiger, J. E. Smerdon, B. I. Cook, R. Seager, A. P. Williams, E. R. Cook, Oceanic and radiative forcing of medieval megadroughts in the American Southwest. *Sci. Adv.* **5**, eaax0087 (2019).
38. E. M. Fischer, U. Beyerle, R. Knutti, Robust spatially aggregated projections of climate extremes. *Nat. Clim. Chang.* **3**, 1033–1038 (2013).
39. A. W. Western, G. Blöschl, R. B. Grayson, Toward capturing hydrologically significant connectivity in spatial patterns. *Water Resour. Res.* **37**, 83–97 (2001).
40. D. L. Schumacher, J. Keune, C. C. van Heerwaarden, J. V.-G. de Arellano, A. J. Teuling, D. G. Miralles, Amplification of mega-heatwaves through heat torrents fuelled by upwind drought. *Nat. Geosci.* **12**, 712–717 (2019).
41. E. M. Fischer, Autopsy of two mega-heatwaves. *Nat. Geosci.* **7**, 332–333 (2014).
42. M. Hauser, R. Orth, S. I. Seneviratne, Role of soil moisture versus recent climate change for the 2010 heat wave in western Russia. *Geophys. Res. Lett.* **43**, 2819–2826 (2016).
43. E. M. Fischer, S. I. Seneviratne, P. L. Vidale, D. Lüthi, C. Schär, Soil moisture–atmosphere interactions during the 2003 European summer heat wave. *J. Climate* **20**, 5081–5099 (2007).
44. D. G. Miralles, A. J. Teuling, C. C. van Heerwaarden, J. V.-G. de Arellano, Mega-heatwave temperatures due to combined soil desiccation and atmospheric heat accumulation. *Nat. Geosci.* **7**, 345–349 (2014).
45. R. J. van der Ent, H. H. G. Savenije, B. Schaefli, S. C. Steele-Dunne, Origin and fate of atmospheric moisture over continents. *Water Resour. Res.* **46**, W09525 (2010).
46. D. Barriopedro, E. M. Fischer, J. Luterbacher, R. M. Trigo, R. García-Herrera, The hot summer of 2010: Redrawing the temperature record map of Europe. *Science* **332**, 220–224 (2011).

47. K. C. Mo, D. P. Lettenmaier, Precipitation deficit flash droughts over the United States. *J. Hydrometeorol.* **17**, 1169–1184 (2016).
48. N. S. Diffenbaugh, M. Ashfaq, Intensification of hot extremes in the United States. *Geophys. Res. Lett.* **37**, L15701 (2010).
49. B. I. Cook, J. E. Smerdon, R. Seager, E. R. Cook, Pan-continental droughts in North America over the last millennium. *J. Climate* **27**, 383–397 (2014).
50. T. Das, D. W. Pierce, D. R. Cayan, J. A. Vano, D. P. Lettenmaier, The importance of warm season warming to western U.S. streamflow changes. *Geophys. Res. Lett.* **38**, L23403 (2011).
51. M. van de Pol, S. Jenouvrier, J. H. C. Cornelissen, M. E. Visser, Behavioural, ecological and evolutionary responses to extreme climatic events: Challenges and directions. *Philos. Trans. R. Soc. B Biol. Sci.* **372**, 20160134 (2017).
52. A. F. Van Loon, K. Stahl, G. D. Baldassarre, J. Clark, S. Rangecroft, N. Wanders, T. Gleeson, A. I. J. M. Van Dijk, L. M. Tallaksen, J. Hannaford, R. Uijlenhoet, A. J. Teuling, D. M. Hannah, J. Sheffield, M. Svoboda, B. Verbeiren, T. Wagener, H. A. J. Van Lanen, Drought in a human-modified world: Reframing drought definitions, understanding, and analysis approaches. *Hydrol. Earth Syst. Sci.* **20**, 3631–3650 (2016).
53. R. B. Nelsen, Properties and applications of copulas: A brief survey. *First Brazilian Conf. Stat. Model. Insur. Financ.* **3**, 1–18 (2003).
54. P. A. P. Moran, The interpretation of statistical maps. *J. R. Stat. Soc. Ser. B* **10**, 243–251 (1948).
55. P. A. Moran, Notes on continuous stochastic phenomena. *Biometrika* **37**, 17–23 (1950).
56. A. Getis, J. K. Ord, The analysis of spatial association by use of distance statistics. *Adv. Spat. Sci.* **61**, 127–145 (2010).
57. H. B. Mann, Nonparametric tests against trend. *Econometrica* **13**, 245 (1945).
58. M. Kendall, Rank correlation. *Nature* **142**, 402 (1938).
59. T. W. Anderson, D. A. Darling, A test of goodness of fit. *J. Am. Stat. Assoc.* **49**, 765–769 (1954).
60. F. J. Massey Jr., The Kolmogorov-Smirnov test for goodness of fit. *J. Am. Stat. Assoc.* **46**, 68–78 (1951).

Acknowledgments: We would like to acknowledge three anonymous reviewers who helped improve the quality of this paper. **Funding:** M.S. is partially supported by NSF award 1840654.
Author contributions: M.S. conceived the idea and developed it with M.R.A. and A.A. M.R.A. conducted all the analyses. M.S. and M.R.A. prepared the first draft of the paper. All authors contributed to the analysis, interpretation of the results, and final draft of the paper.
Competing interests: The authors declare that they have no competing interests. **Data and materials availability:** All data needed to evaluate the conclusions in the paper are present in the paper and/or the Supplementary Materials. Additional data related to this paper may be requested from the authors. Monthly precipitation and temperature data are acquired from the United States Climate Divisional Database through the National Oceanic and Atmospheric Administration (NOAA). The data can be obtained from http://ncdc.noaa.gov/cag/time-series/us.

Submitted 10 September 2019
Accepted 3 August 2020
Published 23 September 2020
10.1126/sciadv.aaz4571

Citation: M. R. Alizadeh, J. Adamowski, M. R. Nikoo, A. AghaKouchak, P. Dennison, M. Sadegh, A century of observations reveals increasing likelihood of continental-scale compound dry-hot extremes. *Sci. Adv.* **6**, eaaz4571 (2020).

Science Advances

A century of observations reveals increasing likelihood of continental-scale compound dry-hot extremes

Mohammad Reza Alizadeh, Jan Adamowski, Mohammad Reza Nikoo, Amir AghaKouchak, Philip Dennison and Mojtaba Sadegh

Sci Adv **6** (39), eaaz4571.
DOI: 10.1126/sciadv.aaz4571